Assessment of arrhythmia mechanism and burden of the infarcted ventricles following remuscularization with pluripotent stem cell-derived cardiomyocyte patches using patient-derived models

Joseph K. Yu [1,2,3,4]*, Jialiu A. Liang [1,2], William H. Franceschi [1,2], Qinwen Huang[1,2], Farhad Pashakhanloo [2], Eric Sung [2,3,4], Patrick M. Boyle [2,5,6,7], and Natalia A. Trayanova [2,3,4]

[1]Institute for Computational Medicine, Johns Hopkins University, 3400 N Charles Street, 208 Hackerman, Baltimore, MD 21218, USA; [2]Department of Biomedical Engineering, Johns Hopkins University, 3400 N Charles Street, 208 Hackerman, Baltimore, MD 21218, USA; [3]Department of Medicine, Johns Hopkins University School of Medicine, Baltimore, MD, USA; [4]Alliance for Cardiovascular Diagnostic and Treatment Innovation (ADVANCE), Johns Hopkins University, 3400 N Charles Street, 216 Hackerman, Baltimore, MD, USA; [5]Department of Bioengineering, University of Washington, Seattle, WA, USA; [6]Institute for Stem Cell and Regenerative Medicine, University of Washington, Seattle, WA, USA and [7]Center for Cardiovascular Biology, University of Washington, Seattle, WA, USA

|	
Aims	Direct remuscularization with pluripotent stem cell-derived cardiomyocytes (PSC-CMs) seeks to address the onset of heart failure post-myocardial infarction (MI) by treating the persistent muscle deficiency that underlies it. However, direct remuscularization with PSC-CMs could potentially be arrhythmogenic. We investigated two possible mechanisms of arrhythmogenesis—focal vs. re-entrant—arising from direct remuscularization with PSC-CM patches in two personalized, human ventricular computer models of post-MI. Moreover, we developed a principled approach for evaluating arrhythmogenicity of direct remuscularization that factors in the VT propensity of the patient-specific post-MI fibrotic substrate and use it to investigate different conditions of patch remuscularization.
Methods and results	Two personalized, human ventricular models of post-MI (P1 and P2) were constructed from late gadolinium enhanced (LGE)-magnetic resonance images (MRIs). In each model, remuscularization with PSC-CM patches was simulated under different treatment conditions that included patch engraftment, patch myofibril orientation, remuscularization site, patch size (thickness and diameter), and patch maturation. To determine arrhythmogenicity of treatment conditions, VT burden of heart models was quantified prior to and after simulated remuscularization and compared. VT burden was quantified based on inducibility (i.e. weighted sum of pacing sites that induced) and severity (i.e. the number of distinct VT morphologies induced). Prior to remuscularization, VT burden was significant in P1 (0.275) and not in P2 (0.0, not VT inducible). We highlight that re-entrant VT mechanisms would dominate over focal mechanisms; spontaneous beats emerging from PSC-CM grafts were always a fraction of resting sinus rate. Moreover, incomplete patch engraftment can be particularly arrhythmogenic, giving rise to particularly aberrant electrical activation and conduction slowing across the PSC-CM patches along with elevated VT burden when compared with complete engraftment. Under conditions of complete patch engraftment, remuscularization was almost always arrhythmogenic in P2 but certain treatment conditions could be anti-arrhythmogenic in P1. Moreover, the remuscularization site was the most important factor affecting VT burden in both P1 and P2. Complete maturation of PSC-CM patches, both ionically and electrotonically, at the appropriate site could completely alleviate VT burden.
Conclusion	We identified that re-entrant VT would be the primary VT mechanism in patch remuscularization. To evaluate the arrhythmogenicity of remuscularization, we developed a principled approach that factors in the propensity of the

* Corresponding author. Tel: +1 682 561 6161; E-mail: jyu78@jhmi.edu

patient-specific fibrotic substrate for VT. We showed that arrhythmogenicity is sensitive to the patient-specific fibrotic substrate and remuscularization site. We demonstrate that targeted remuscularization can be safe in the appropriate individual and holds the potential to non-destructively eliminate VT post-MI in addition to addressing muscle deficiency underlying heart failure progression.

Graphical Abstract
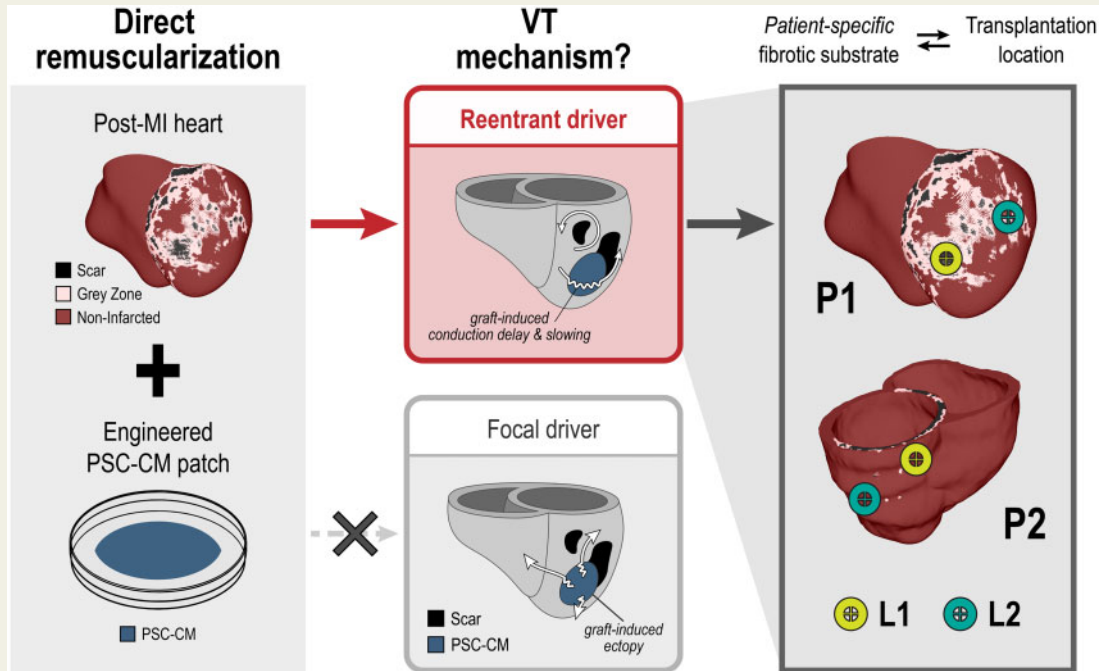
1. Introduction

Persistent muscle deficiency underlies systolic heart failure (HF) progression post-myocardial infarction (MI) and remains unaddressed. Attributable to low cardiomyocyte turnover (<1% annually) in the adult human ventricles,[1,2] persistent muscle deficiency post-MI can cause chronic mechanical overload that contributes to pathological remodeling and worsening contractile function of the surviving myocardium. Consequently, nearly 20% of post-MI patients over the age of 45 will progress towards HF in 5 years.[3] In end-stage HF, heart transplantation remains the best treatment option to date despite an extreme shortage of donor hearts.[4] The urgent need for regenerative therapies that address post-MI muscle deficiency is growing as the global prevalence of post-MI HF continues to rise.[3]

Direct remuscularization is one promising regenerative approach to treat post-MI muscle deficiency. In this approach, exogenous cardiomyocytes (CMs) are introduced to replace those lost during MI.[5–9] Systolic contraction is enhanced by the integration of these graft myocytes with that of the host ventricular myocardium. Pluripotent stem cell-derived cardiomyocytes (PSC-CMs) have typically been used because of their wide availability.[10–12] Delivery of PSC-CMs into the post-MI ventricles has been accomplished either through intramyocardial injection[13–16] or

transplantation of engineered myocardial patches.[17–22] In intramyocardial injection, cultured PSC-CMs are first dissociated and suspended in solution before injection; to create myocardial patches, PSC-CMs are integrated into synchronously beating tissues prior to transplantation. Both modalities have demonstrated PSC-CM engraftment, decreased infarct size, and instances of improved ventricular contractility.[13,17,23] PSC-CMs have also been observed to morphologically mature[13,22,24,25] *in vivo*. Compared with intramyocardial injection however, myocardial patch transplantation has resulted in higher PSC-CM viability and engraftment.[17,20,21]

Regardless of delivery modality, graft-induced arrhythmias pose a critical concern but remain difficult to study *in vivo*. *In vivo* reports of graft-induced VT, a life-threatening heart rhythm disorder, have been inconsistent. While some pre-clinical large animal model studies have observed alarmingly high rates of VT,[13,14,26] others have not.[17,23] Direct remuscularization with PSC-CMs in small animal model studies has been found to not be arrhythmogenic[20,27] and to be potentially even anti-arrhythmic.[15] These inconsistent findings can be partially attributed to the fact that infarct geometry and size cannot be precisely controlled experimentally. The individualized heterogeneous distribution of infarcted tissue itself can promote the initiation and maintenance of re-entrant VT post-MI[28,29] prior to remuscularization. The current methodology of
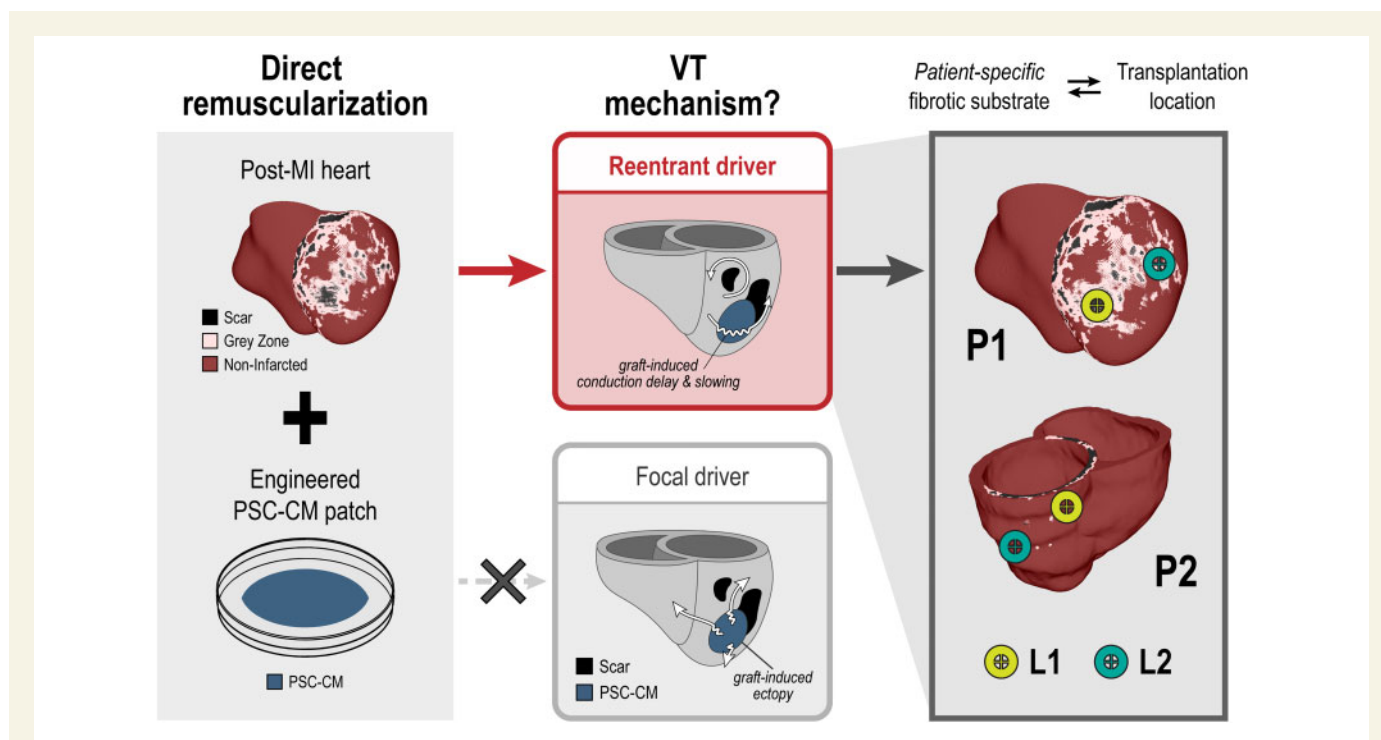
Figure 1 Study overview. Patient-specific, post-MI ventricular heart models (left) derived from LGE-MRIs with biophysically detailed representations of non-infarcted (maroon), peri-infarcted grey zone (pink), and scar (black) myocardial regions were used to study the arrhythmia consequences of direct remuscularization with engineered pluripotent stem cell-derived cardiomyocyte (PSC-CM) patches (blue). When the transplantation and integration of PSC-CM patches onto the post-MI models were simulated, re-entry (top middle) was identified as the primary driver of ventricular arrhythmia as opposed to focal ectopy (bottom middle) arising from intrinsic PSC-CM automaticity. Arrhythmogenicity of remuscularization was closely linked to both the transplantation site and the patient-specific post-MI fibrotic substrate (right).

comparing VT across pooled control and treatment groups is inexact because the contribution of the individual post-MI substrate pre-remuscularization is not considered in the treated group; this uncertainty is exacerbated by the weak statistical power of most pre-clinical large animal studies. Moreover, the long-term arrhythmia consequences of partial remuscularization with PSC-CMs remain to be thoroughly studied; how to modify the myocardial substrate (i.e. distribution of infarcted tissue) with graft myocardium in a way that minimizes risk and burden for re-entrant VT also remains unknown.

In this three-dimensional (3D) computational study, we aimed to address three principal knowledge gaps. *Figure 1* presents an overview of the study and our findings. Firstly, we simulated remuscularization with PSC-CM patches (left) and sought to determine whether focal vs. re-entrant VT mechanisms dominate (middle). Spontaneously beating PSC-CMs have been observed to generate regular ectopic beats when injected intramyocardially into the ventricles.[30] However, it remains unknown whether a graft-induced, focal mechanism or a re-entrant mechanism would drive VT in the context of patch remuscularization. After we identified that re-entry would be the primary VT driver, we next sought to determine whether the patient-specific post-MI substrate would affect the emergence of graft-induced re-entrant VT in remuscularization with PSC-CM patches (right). We studied this in two 3D biophysically detailed, personalized human ventricular models (P1, P2) of post-MI with distinctly different infarct size, geometry, and accompanying VT burden; models were constructed from clinical late gadolinium enhanced (LGE)-magnetic resonance images (MRIs).[28] Thirdly and lastly, we sought to determine how different remuscularization treatment conditions (i.e. location, patch size, fibre orientation) altered VT burden and dynamics of re-entry. A principled approach was developed to determine arrhythmogenicity of PSC-CM patch remuscularization across different treatment conditions by comparing VT burden following simulated treatment to that of baseline. We present evidence that the patient-specific fibrotic substrate together with the site of remuscularization plays a role in the arrhythmogenicity of remuscularization (right). While optimality of remuscularization—both identifying the appropriate candidate and the appropriate treatment conditions—remains an open question, our proposed methodology enables the exploration of arrhythmogenicity that complements *in vivo* investigations. Our approach demonstrates the utility of biophysical human models in addressing the safety of remuscularization therapy and providing a bridge between pre-clinical animal studies and human clinical trials.

2. Methods

2.1 Modelling remuscularization with PSC-CM patches in clinical LGE-MRI-based human post-MI heart models

Remuscularization with PSC-CM patches was studied in two different 3D personalized models of the post-MI ventricles to determine how arrhythmogenicity of remuscularization is affected by the patient-specific post-MI substrate. For the two personalized heart models, the Johns

Hopkins Institutional Review Board (IRB) approved sharing of de-identified patient data; the IRB did not require patient informed consent given the retrospective nature of the study. Full details of the 3D model reconstruction process and electrophysiology modelling can be found in previous publications by our group.[28,31] Briefly, boundaries of the myocardial wall were first manually contoured for each MRI stack; non-infarcted, grey zone, and scar regions in the myocardium were delineated by signal thresholding. The wall contours and regions were then merged to create the final geometric ventricular reconstruction. Fibre orientations were assigned in each geometric model using a previously validated rule-based approach.[32] In non-infarcted myocardium regions, human ventricular cardiomyocyte membrane kinetics were simulated using the ten Tusscher–Panfilov formulation.[33] Modifications to the ionic model were incorporated to represent electrophysiological remodelling in grey zone myocardium. Infarcted myocardium was modelled as non-conducting and unexcitable. Tissue conductivities in non-infarcted and grey zone myocardium were assigned as previously described[28,31] with appropriate adjustments incorporated into the latter to reflect connexin-43 (Cx43) remodelling observed experimentally. Electrical wave propagation in 3D heart models was governed by the monodomain formulation; all simulations were executed with the CARP software package[34,35] on a parallel computing system.

Transplantation and engraftment of PSC-CM patches were modelled as follows. Myocardial patch transplantation, compared with intramyocardial injection, can only occur along the epicardium and cell migration is minimal because PSC-CMs are first integrated into confluent sheets *in vitro*.[17,20,22] In each heart model, PSC-CM patches were circular in shape and transplanted onto the ventricular myocardium below the epicardium enabling direct interfacing between host and graft. Access to the myocardium below the epicardium has been clinically reported,[36,37] but details regarding how this has been achieved experimentally *in vivo* across several published studies remain limited.[17,21,38] Simulating myocardial patch transplantation and engraftment was accomplished in three steps. First, all points along the epicardium of the finite element mesh were first identified. Next, the subset of points within a specified distance from a centering point specified the size and location of the patch. Finally, all elements with a vertex that included at least one of these points were identified and thus completely specifying the PSC-CM patch region. Patch thickness was varied across 300 μm, 1 mm, and 2 mm. However, 300 μm represents the limits of what has been experimentally accomplished with purely PSC-CM patches to date.[17,21,38] Unless otherwise specified, PSC-CM patch myofibres were assumed to be aligned to that of adjacent myofibres in the host myocardium. Alignment of PSC-CMs has been observed to contribute to anisotropic conduction in patches *in vitro*[18,39] much like how alignment of ventricular cardiomyocytes contributes to anisotropic conduction *in vivo*.[40,41] To study the consequences of misaligned PSC-CM myofibres, patch fibre orientations were altered. In cases where patch fibres were aligned but not properly oriented with the local host myofibres, patch fibres were rotated ±45° or ±90° with respect to the surface normal of the nearest epicardial element face. In cases where patch fibres were not aligned, fibres were randomly rotated (rotation angles were sampled from a uniform distribution between ±90°) with respect to the surface normal of the nearest epicardial element face.

Membrane kinetics in the PSC-CM patches were represented by the Paci et al.[42] formulation for a ventricular-like, human-induced pluripotent stem cell-derived cardiomyocyte (hiPSC-CM)[42]; this subtype was selected because it is the most appropriate for remuscularization of the ventricles. Unless otherwise specified, tissue conductivities in PSC-CM patches were 10% of that in normal myocardium; this is because PSC-CM patches cultured *in vitro* have lower levels of Cx43 expression and noticeably slower conduction velocity (CV) compared with native ventricular myocardium.[18] Lastly, we simulated cases of complete and partial patch engraftment. In the former (Supplementary material online, *Figure S1A*), electrotonic coupling between the host and graft was assumed to be determined by the composition of the underlying myocardial substrate (i.e. non-infarcted, grey zone, or scar). In the latter, however, electrical coupling of the transplanted PSC-CM patch and host myocardium is just beginning to form[43] and is distinct from either. To simulate this, conductivity between the graft and host myocardium was both isotropic and reduced (magnitude of transverse conductivity of non-infarcted myocardium). This interface (one-element thick) did not have any specified membrane kinetics despite having a distinct electrical conductivity (Supplementary material online, *Figure S1B*). Ultimately however, nodal assignment of ionic properties remained identical across both simulated conditions of complete and partial engraftment.

2.2 Quantifying re-entrant VT burden and determining arrhythmogenicity

The burden for re-entrant VT was quantified using a newly defined metric called the VT burden score (VBS) in each heart model across each simulated remuscularization treatment condition. We defined VBS as the product of two measured summary statistics: inducibility and severity. These statistics were computed from results obtained using our previously published Virtual-heart Arrhythmia Risk Predictor (VARP) protocol.[28,31] In VARP, patient-specific ventricular models were subjected to simulated pacing from 19 uniformly distributed endocardial sites (2 in the right ventricle and 17 in the LV) in an attempt to induce re-entrant VTs. Pacing locations were automatically assigned[44] in the LV based on the AHA LV segments.[45]

From the simulation results, inducibility and severity were computed as follows. Inducibility, a measure of VT susceptibility, was computed as the weighted sum of all instances of induced re-entrant VT normalized by the total number of pacing sites (19). The weight for each instance of induced VT was the reciprocal of the number of premature stimuli required to induce VT (at most 4). Bounded between 0 and 1, inducibility can be thought of as a probability for VT induction in response to pacing in the heart model. Severity represented the number of unique re-entrant VT morphologies that could be induced in each personalized model. VT morphologies were determined in a semi-automated fashion using pseudo-ECGs as outlined below.

The VBS of models at baseline and after simulated remuscularization under various conditions were compared to determine arrhythmogenicity of treatment. A treatment condition was arrhythmogenic if its corresponding VBS was elevated compared with that at baseline.

2.3 Semi-automated determination of unique VT morphologies

Unique VT morphologies were determined quantitatively by comparing pseudo-ECGs from the final two seconds of simulation if re-entrant VT was induced. To compute pseudo-ECGs, lead positions around the heart were determined with respect to the heart geometry and its anatomical orientation. A schematic of lead positioning and description of bipolar pseudo-ECG lead computation is shown in Supplementary material online, *Figure S2*. To compare pseudo-ECGs, traces were first aligned by determining the time lag that minimized the sum-squared differences. VT morphologies were considered the same if the sum-squared difference

was less than 100; morphologies were considered distinct if the sum-squared difference exceeded 300. VT morphologies were manually inspected to determine uniqueness if the sum-squared differences were between 100 and 300. All distinct VT morphologies following patch remuscularization can be found in the Supplementary material online (*Figure S4* for P1 and *Figure S5* for P2).

3. Results

3.1 Characterization of baseline VT burden in P1 and P2

VT burden was characterized in the two patient-specific models (P1 and P2) at baseline prior to simulated remuscularization. This baseline was used to provide an accurate determination of arrhythmogenic remuscularization conditions. While P1 had large infarct that spanned most of the anterior LV as well as the septum, P2 had a moderate infarct localized to the posterior superior LV (*Figure 2A*). VT was induced from three pacing sites in P1 (*Figure 2A*, top), two of which induced on S3 and one on S4. Contrarily, P2 was not inducible for VT (*Figure 2A*, bottom). In P1, all induced VT morphologies were distinct (*Figure 2B*). In morphology B1

(*Figure 2B*, top), re-entrant waves revolved clockwise anchoring along scar in the lateral LV; a bystander wave propagated around the scar in the basal anterior LV. In morphology B2 (*Figure 2B*, middle), a figure of eight re-entry anchored around the scar in the apical anterior and lateral LV. A double figure of eight characterized morphology B3 (*Figure 2B*, bottom); one of the figure of eight re-entries anchored at scar in the basal anterior LV near the septum, while the other anchored along the apical anterior LV wall. In total, the baseline inducibility and VT burden of P1 were 0.0917 and 0.275, respectively. P2's baseline inducibility and VT burden were both 0.0. These are summarized in *Figure 2C and D*, respectively.

3.2 Re-entrant mechanisms dominate over focal mechanisms in patch remuscularization

In the first set of experiments, we sought to identify the primary cause of arrhythmia in direct remuscularization of the infarcted ventricles with PSC-CM patches. Specifically, whether VTs would be driven or sustained by graft-induced focal ectopy or re-entry. We tested the former hypothesis using an idealized contiguous PSC-CM graft with finite volume ($0.344 \pm 0.035 \, cm^3$) (*Figure 3A*). The rate of graft-induced spontaneous
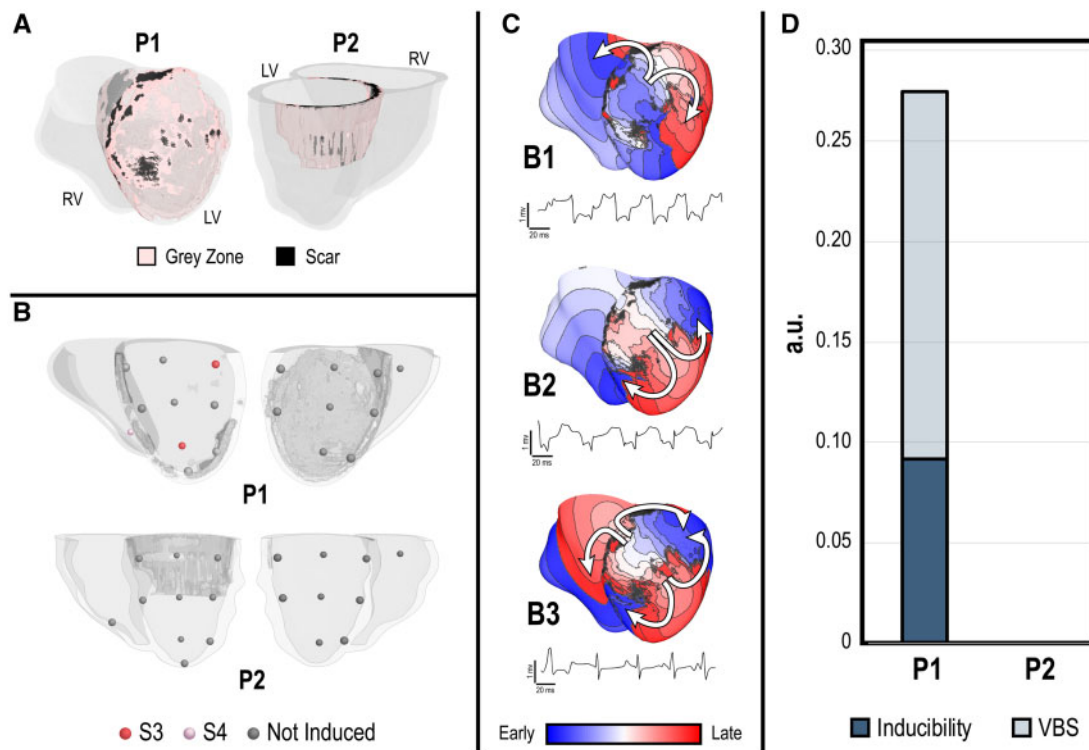
Figure 2 VT burden in P1 and P2 at baseline prior to simulated remuscularization. (*A*) Infarct regions (peri-infarct grey zone in pink, scar in black) of P1 and P2 are visualized with semi-transparent non-infarcted regions. Left (LV) and right (RV) ventricle chambers are labelled. While P1 exhibited a large anterior LV infarct that extended into the septum, P2 exhibited a moderate posterior, superior LV infarct. (*B*) Inducibility maps of P1 (top) and P2 (bottom) indicate the outcome of rapid pacing at each endocardial pacing site (19 total). In P1, VT was induced from three pacing sites, two on S3 (red) and one on S4 (pink). In P2, VT was not induced. (*C*) Activation maps and pseudo-ECG traces are shown for the three distinct VT morphologies (B1, B2, and B3) induced in P1 at baseline. Activation map colours indicate the sequence of electrical excitation from early (blue) to late (red) for one cycle of re-entry. Pseudo-ECGs show the electrical waveforms for each distinct VT morphology across time. (*D*) Bar graphs of VT burden in P1 and P2 at baseline; inducibility is overlaid on the VT burden score (VBS). P1 had significant VT burden (VBS = 0.275, inducibility = 0.917, severity = 3), while P2 had none (VBS = inducibility = severity = 0).
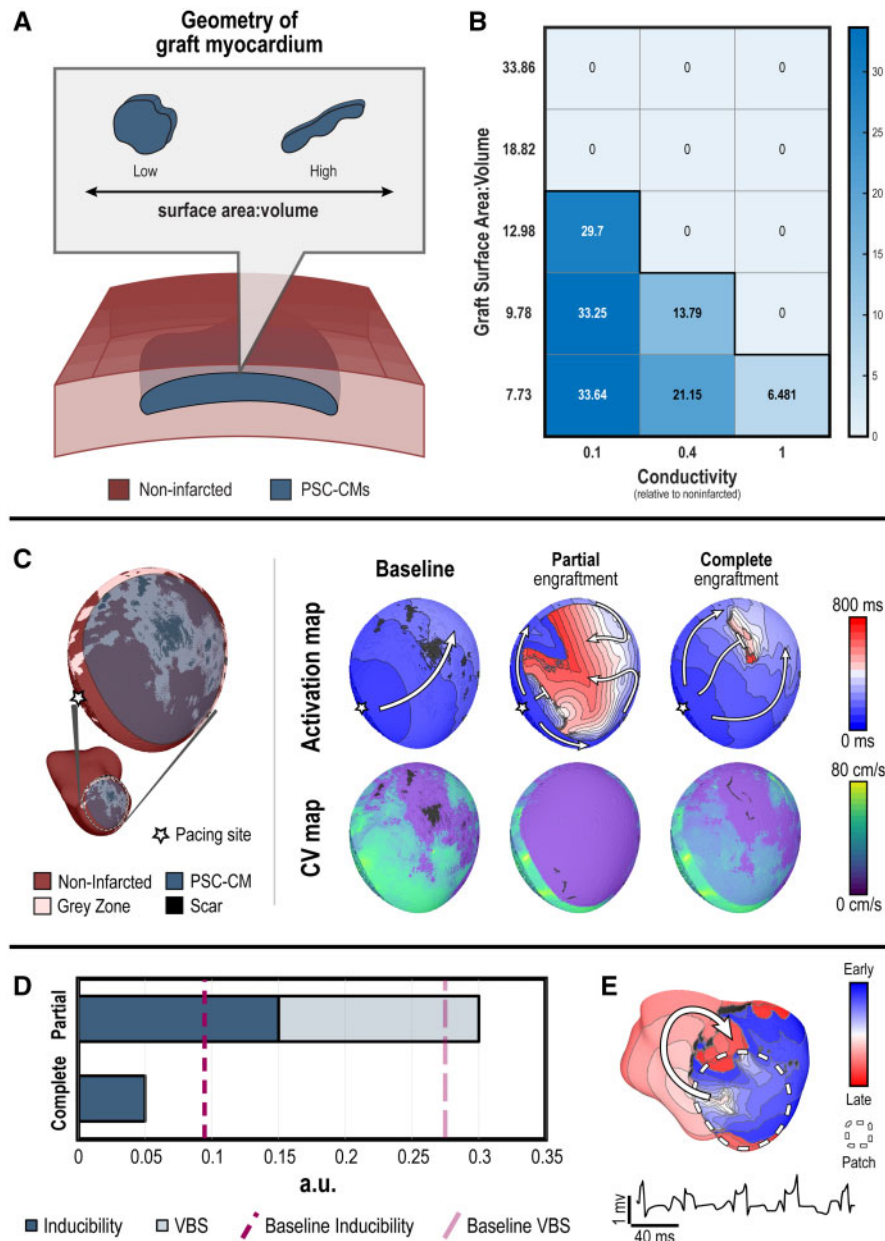
Figure 3 A re-entrant VT mechanism dominates over a focal mechanism in patch remuscularization, but partial engraftment of PSC-CM patches exacerbates VT burden due to conduction slowing through the patch. (*A*) Schematic of experimental set-up. The emergence and rate of focal ectopic propagations from graft myocardium was observed for PSC-CMs embedded within a cut-out of the ventricular myocardial wall; the surface area-to-volume ratio of the graft was altered. (*B*) Frequency (b.p.m.) of graft-induced focal ectopic propagations across different graft geometries (i.e. surface area: volume ratio) and conductivities. (*C*) Remuscularization with a PSC-CM patch (radius = 3.2 cm) applied to segment of infarct (L1) along the anterior, inferior LV of P1 (left inset) was simulated; simulated pacing occurred at the starred site. Electrical propagation across the patch was observed under baseline (left), partial engraftment (middle), and complete engraftment (right); activation maps (top) and conduction velocity maps (bottom) indicate the sequence of epicardial electrical activation and local conduction velocity, respectively. (*D*) Bar graph of inducibility (dark blue) and VT burden (VBS, light blue) for P1 under conditions of partial and complete engraftment; dashed lines indicate inducibility (dark pink) and VT burden (light pink) at baseline. (*E*) Activation map and pseudo-ECG of the single emergent VT morphology induced in P1 when complete engraftment was simulated.

ectopic propagations was quantified across a range of graft myocardium conductivities (10%, 40%, and 100% relative to non-infarcted myocardium) and interfacing surface area between host and graft myocardium. The frequency of graft-induced ectopic propagations was reduced by either increasing coupling between PSC-CMs within the graft or increasing the interface area between host and graft myocardium (*Figure 3B*). However, the frequency of ectopic beats never exceeded the intrinsic automaticity of individual PSC-CMs (~37.5 b.p.m.). This highlights how source-sink effects between host and graft myocardium alter the emergence and frequency of graft-induced ectopic beats; ventricular

myocytes in the host myocardium can act as a strong electrotonic sink to suppress the intrinsic automaticity of PSC-CMs in the graft. Because PSC-CM patches have a larger surface area-to-volume ratio, they did not exhibit spontaneous beating. In the context of patch remuscularization, we concluded that focally driven VTs arising from the intrinsic automaticity of PSC-CMs were unlikely and that a re-entrant driver VT mechanism would be more plausible.

With this established, we next hypothesized that partial PSC-CM patch engraftment following transplantation could be especially arrhythmogenic because of conduction delay at the host–graft interface. This could be a transient phenomenon that occurs during the natural progression of host–graft coupling or could be persistent if fibrosis were to develop at the host–graft interface. We tested this in P1, where we simulated remuscularization with a PSC-CM patch along the apical anterior LV, a representative site directly over the infarct (*Figure 3C*). The radius of the patch was 3.2 cm, slightly smaller than the largest patches investigated *in vivo*.[17] When P1 was electrically paced, electrical activation and CV across the PSC-CM patch under conditions of partial and complete engraftment were studied and compared with those at baseline prior to remuscularization. Compared with baseline (*Figure 3C*, top left), electrical activation was significantly delayed under partial PSC-CM patch engraftment (*Figure 3C*, top middle). Electrical waves initially failed to propagate across the PSC-CM patch proximal to the pacing site (indicated by star), which gave rise to subsequent retrograde electrical propagation. CV maps indicated that CV was depressed across the entire PSC-CM patch (*Figure 3C*, bottom middle vs. bottom left). Contrarily, electrical activation across the PSC-CM patch when engraftment was complete was very similar to that at baseline (*Figure 3C*, top right vs. top left); bidirectional conduction block and conduction slowing occurred distal to the pacing site where the PSC-CM patch covered a larger region of scar. Additionally, local CV across the PSC-CM patch was significantly faster and mirrored that of the underlying host myocardial substrate (*Figure 3C*, bottom right vs. bottom left). CV was faster in regions adjacent to non-infarcted myocardium and slower in regions adjacent to grey zone myocardium, indicating that the electrical activation of host myocardium drove electrical propagation across the PSC-CM patch. Therefore, partial patch engraftment had the additional effect of reducing CV through the patch; electrical propagation through the patch became reliant on poor coupling between PSC-CMs.

Consequently, VT burden of P1 was elevated under conditions of partial patch engraftment when compared with baseline (*Figure 3D*). In total (*Figure 3D*), inducibility and VT burden of P1 under conditions of partial engraftment were 0.15 and 0.30, respectively; under conditions of complete engraftment, inducibility and VT burden were much lower (0.05) and surprisingly lower than those of baseline. Under conditions of partial engraftment, VT was induced from three pacing sites, all on S2. Two distinct VT morphologies were detected (Supplementary material online, *Figure S6*). One of the morphologies resembled the baseline morphology B2 (Supplementary material online, *Figure S6*, top). While the other morphology initially resembled B2 as well (Supplementary material online, *Figure S6*, bottom), subsequent figure of eight re-entrant waves moved around infarcted regions of the anterior LV; host–graft conduction delays contributed to these meandering breakthroughs. Under conditions of complete engraftment however, VT was only induced from 1 pacing site on S2. The VT morphology (*Figure 3E*) was emergent (E6, see Supplementary material online for all annotated morphologies); re-entrant waves anchored to scar along the anterior LV near the septum and propagated through the patch.

Overall, we demonstrated that a re-entrant mechanism dominates over a focal mechanism in patch remuscularization. Moreover, we highlighted how partial engraftment of myocardial tissues can elevate arrhythmogenic propensity by contributing to conduction delay between host and graft myocardium as well as conduction slowing by unmasking poor electrotonic coupling between PSC-CMs in the graft. The next sections will explore the relative importance of various other parameters under conditions of complete engraftment. Annotations of all observed VT morphologies can be found in the Supplementary material online.

3.3 Complete engraftment: transplantation location has a dominant effect on VT burden

In the first set of simulation experiments under conditions of complete engraftment, we sought to determine whether VT burden is affected primarily by transplantation location or cell orientation. Myofibrils in the ventricles rotate from endocardium to epicardium and preferential conduction occurs along the myofibrils.[32] Similarly, anisotropic conduction in patches can arise from PSC-CM alignment induced through micropatterning.[18] Remuscularization with PSC-CM patches (radius = 3.2 cm) was simulated at two different locations (L1, L2) along the infarct in both P1 and P2 (*Figure 4A*). In P1 (*Figure 4A*, top), L1 was located along the apical anterior LV, while L2 was along the lateral LV free wall. In P2 (*Figure 4A*, bottom), L1 was located along the basal inferior LV, while L2 was along the lateral LV free wall. L1 was centrally located over the infarct, while L2 straddled infarcted and non-infarcted myocardium. The rationale for the latter is that improved perfusion from host vasculature in non-infarcted myocardium can boost PSC-CM patch viability.[13,46] Five different PSC-CM myofibril orientations were simulated for each site: 0°, ±45°, and 90° orientations relative to the native myofibrils in conditions of anisotropic conduction and random myofibrils under isotropic conduction.

In P1, remuscularization at L1 resulted in VT induction and corresponding VT burden of 0.05 regardless of PSC-CM myofibril orientation (*Figure 4B*, left). Remuscularization at L2, however (*Figure 4B*, right), resulted in significantly elevated VT inducibility (mean = 0.112) and VT burden (mean VBS = 0.278) that fluctuated with different PSC-CM myofibril orientations. Inducibility and VT burden changed with different myofibril conditions without an obvious relationship to degree of misalignment. Compared with baseline, remuscularization at L1 reduced both inducibility and VT burden. Contrarily, remuscularization at L2 either increased or did not change inducibility and VT burden compared with baseline. Elevated VT burden at L2 was due in part to an increase in the number of distinct VT morphologies (*Figure 4D*). A single emergent VT morphology was observed when remuscularization occurred at L1. However, numerous VT morphologies were observed when remuscularization occurred at L2, including one observed at baseline and several emergent ones. Specifically, remuscularization at L1 gave rise to the emergent morphology E6 (*Figure 4E*). At L2, the baseline B2 and emergent E7 morphologies were the most prevalent.

In P2, remuscularization at L1 was sensitive to transplantation orientation but not conduction anisotropy (*Figure 4C*, left). Inducibility and VT burden were 0.0263 and 0.0526, respectively, for myofibril orientations 0°, ±45°, and random. For myofibril orientation 90°, inducibility and VT burden were 0.0132. Remuscularization at L2 resulted in an inducibility and VT burden of 0.0132 regardless of patch myofibril orientations (*Figure 4C*, right). Compared with baseline, remuscularization at both
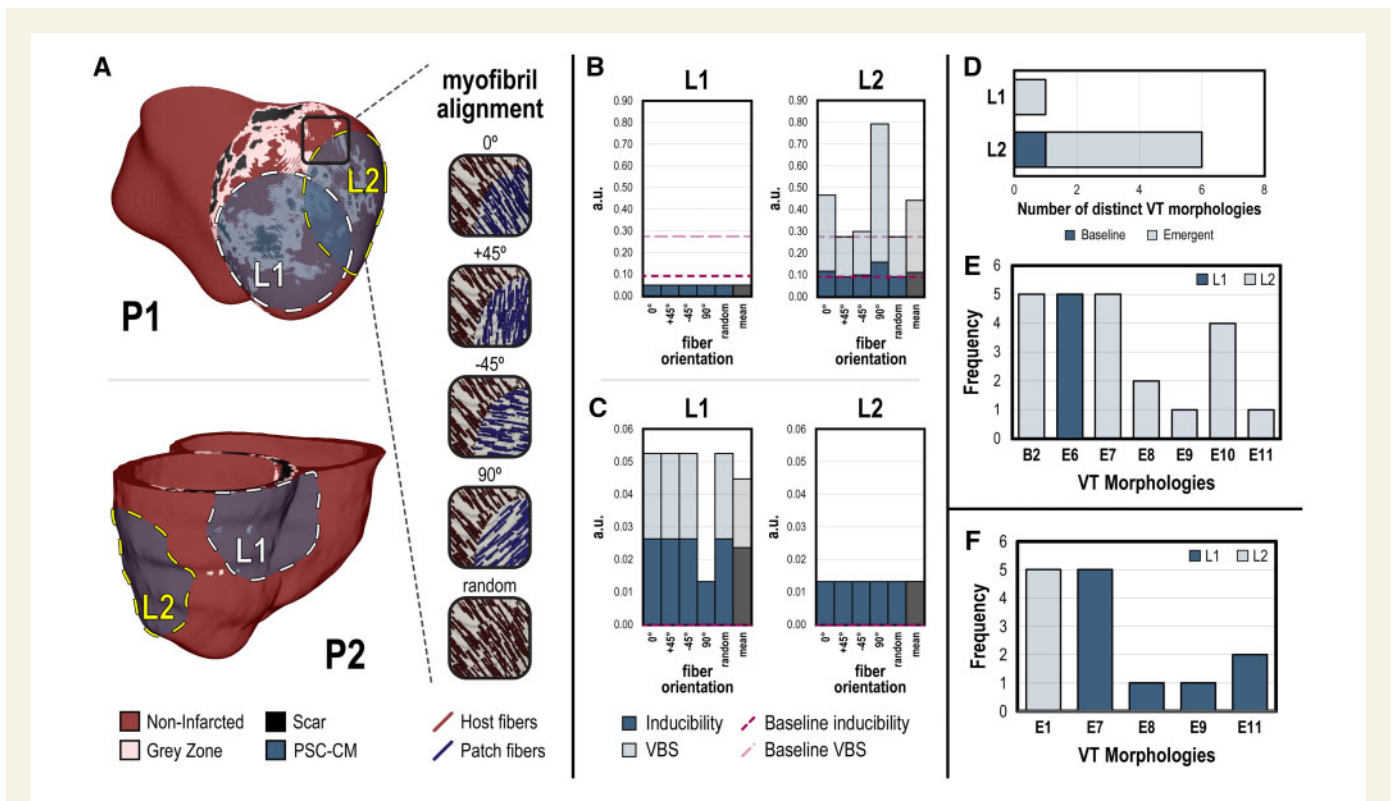
Figure 4 VT burden is more affected by transplantation location compared with patch myofibril alignment. (*A*) Complete engraftment of PSC-CM patches (radius = 3.2 cm) was simulated at two different epicardial sites (L1 and L2) in P1 (top) and P2 (bottom). L1 was centrally located over the infarct, while L2 straddled infarct and non-infarcted myocardium. For each site, different myofibril alignments in PSC-CM patches (0°, ±45°, 90°, random) were simulated. Bar graphs show inducibility (dark blue, overlaid) and VT burden (light blue) for each transplantation site, L1 (left) and L2 (right), across all patch myofibril orientations for (*B*) P1 and (*C*) P2; mean inducibility and VT burden of all myofibril alignments are shown in grey. Dashed lines indicate inducibility (dark pink) and VT burden (light pink) at baseline. (*D*) Number of distinct VT morphologies observed in P1 across all myofibril alignments when remuscularization occurred at L1 compared with L2; emergent morphologies are distinguished from ones observed at baseline. (*E*) All unique VT morphologies and the frequency they were induced in P1. In total, seven different unique morphologies were induced ranging from one previously observed at baseline (B2) to numerous emergent ones (E6, E7, E8, E9, E10, and E11). Complete VT morphology annotations can be found in the Supplementary material online (*F*) All unique VT morphologies and the frequency they were induced in P2.

sites elevated VT burden but more so at L1. Analysis of the emergent VT morphologies induced (*Figure 4F*) indicateed that more distinct VT morphologies were observed when remuscularization occurred at L1 (E7, E8, E9, E11) as opposed to L2 (E1).
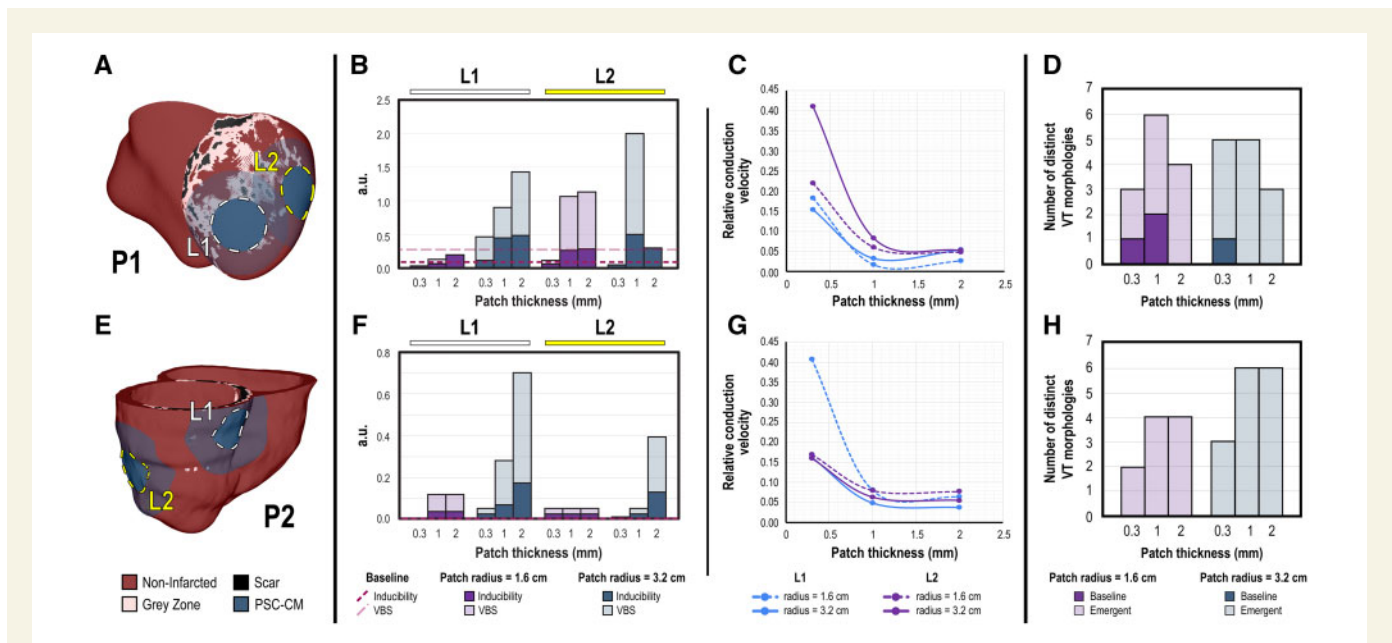
3.4 Complete engraftment: increasing patch thickness exacerbates conduction slowing and VT burden as compared with patch diameter

The effect of cell dosing on arrhythmogenesis has yet to be explicitly investigated in published pre-clinical large animal studies. In our next set of simulations, the dosing effect of PSC-CM remuscularization was investigated by altering patch size. PSC-CM patches with different radii (1.6 and 3.2 cm) and thicknesses (0.3, 1, and 2 mm) were simulated at both sites L1 and L2 in P1 (*Figure 5A*) and P2 (*Figure 5E*). The generation of viable, thick myocardial tissues is limited by the ability to create and integrate dense vascular networks to date, however.[17] PSC-CMs were aligned and properly oriented to the local myofibres (i.e. 0°). We made this decision based on the preceding results and the fact that transplanted PSC-CMs

have been observed to ultimately align with the local host myofibres.[13,17,26]

Inducibility and VT burden changed in a site-dependent manner in response to altered patch dimensions in both P1 and P2 (*Figure 5B and F*, respectively). Consistent across all sites for both P1 and P2 however, inducibility and concomitantly VT burden almost always increased when patch thickness was increased regardless of patch radii. At L1 in P1 and across all patch thicknesses (*Figure 5B*), VT burden was notably reduced relative to baseline (light pink-dashed line) when patch radius was 1.6 cm. This was not the case when patch radius was 3.2 cm or when remuscularization occurred at L2; increasing patch thickness from 0.3 increased VT burden beyond that of baseline. Increased inducibility with increased patch thickness was driven in part by the fact that CV through the PSC-CM patch was reduced in thicker patches for both P1 and P2 (*Figure 5C and G*, respectively). This suggested that electrotonic interactions with the host myocardium can accelerate impulse propagation through the patch. Across both P1 and P2 (*Figure 5D and H*, respectively), the number of distinct VT morphologies did not noticeably correlate with patch depth or radii. The number of VT morphologies in P2 increased when patch thickness or radius was increased; this was not the case in P1, however. Details regarding VT morphologies across different

Figure 5 VT burden increases when PSC-CM patch thickness is increased. (*A, E*) Complete engraftment of PSC-CM patches with different radii (*r* = 1.6 and 3.2 cm) and thicknesses (depths = 0.3, 1, and 2 mm) was simulated at sites L1, L2 in (*A*) P1 and (*E*) P2; patch myofibres were aligned to the local myofibres (i.e. 0°). (*B, F*) Inducibility and VT burden of (*B*) P1 and (*F*) P2 for each transplantation site, (L1, left and L2, right) and for patches with smaller (purple) compared with larger (blue) radii across different patch thicknesses. (*C, G*) Normalized conduction velocity (relative to that of non-infarcted myocardium) vs. patch thickness for different transplantation sites and patch radii in (*C*) P1 and (*G*) P2. (*D, H*) Number of distinct VT morphologies across different patch radii and thicknesses in (*D*) P1 and (*H*) P2.

patch dimensions for P1 and P2 are annotated in Supplementary material online, Tables S1 and S2, respectively.

3.5 Complete engraftment: changes in VT burden is specific to transplantation location during simulated PSC-CM patch maturation

In the final set of experiments, we sought to determine how the maturation of PSC-CM patches altered dynamics of inducibility and VT burden. Maturation of electromechanical coupling between PSC-CMs enable synchronized spontaneous contractions of patches *in vitro*; CV has also been observed to increase across myocardial patches with time spent in culture.[47] Several studies have also indicated that PSC-CMs can ionically and morphologically mature *in vivo*.[22–24,26] However, complete PSC-CM maturation *in vitro* has remained elusive despite numerous efforts to replicate the process of *in vivo* maturation.[47–49] Because a comprehensive and detailed ionic characterization of maturing PSC-CMs has yet to be published, our ability to model intermediate stages of ionic PSC-CM maturation was limited. Therefore, maturation of PSC-CM patches was modelled in four stages (*Figure 6A*). In the first three stages, maturation of electrotonic gap junctional coupling alone was simulated; myofibril conductivities were increased from 10% to 40% and 100% of that of normal myocardium. In the fourth and final stage, membrane kinetics of PSC-CM patches were modelled by that of non-infarcted myocardium. This set-up would allow us to test how inducibility and VT burden could be affected by patch maturation state as well as how they could reasonably evolve *in vivo*. Remuscularization with PSC-CM patches (radius = 3.2 cm) was again simulated at sites L1 and L2, in patients P1 and P2 like before

(*Figure 4A*); myofibres in patches were aligned to those of local host myofibres (i.e. 0°).

Inducibility and VT burden evolved in a site-dependent manner in response to simulated maturation of PSC-CM patches in both P1 (*Figure 6B*) and P2 (*Figure 6D*). In P1, progression from maturation stages 1 to 3 did not alter inducibility or VT burden when remuscularization was simulated at L1 (*Figure 6B*, left); both remained at 0.05. At stage 4 maturation where the patch was modelled as non-infarcted myocardium, P1 was no longer inducible for VT (inducibility and VT burden = 0). At L2 however, progression from maturation stages 1 to 3 increased inducibility and VT burden (*Figure 6B*, right). Inducibility and VT burden were at a maximum at stage 2 (0.158 and 0.792, respectively). At stage 3, inducibility and VT burden remained slightly elevated compared with stage 1 (0.117 and 0.467 compared with 0.125 and 0.500, respectively). Unlike at L1, P1 remained inducible for VT at stage 4 maturation; inducibility and VT burden were dramatically reduced (both 0.025), however. At L1, the number of distinct VT morphologies did not change across maturation stages 1 through 3 (*Figure 6C*, left). At L2 however, the number of distinct VT morphologies changed across maturation stages 1 through 3 (*Figure 6C*, right). Four distinct VT morphologies were observed (three emergent and one baseline) at stages 1 and 3. At stage 2, five distinct VT morphologies were observed (4 emergent and 1 baseline). Only a single morphology was observed at stage 4. In P2, progression from maturation stages 1 through 3 did not alter inducibility or VT burden when remuscularization was simulated at L1 (*Figure 6D*, left; 0.0263 and 0.0526, respectively) or L2 (*Figure 6D*, right; both 0.0132). For stage 4 maturation at L1, inducibility and VT burden of P2 were both 0.0132. P2 was no longer inducible for VT for stage 4 maturation at L2. At L1, two distinct VT morphologies were observed across maturation stages 1 through 3 (*Figure 6E*, left); at stage 4, only a single distinct VT morphology
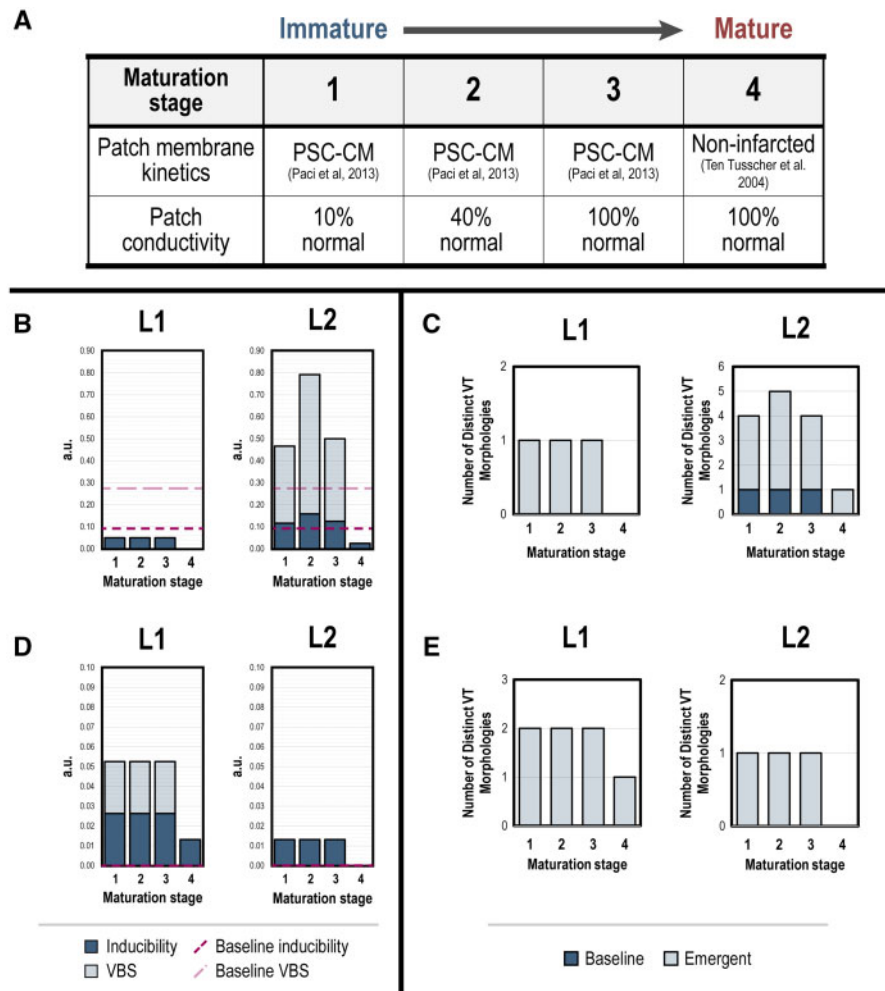
Figure 6 Changes in VT burden during simulated maturation of PSC-CM patches is specific to transplantation location. (*A*) Schematic of simulated PSC-CM patch maturation across four stages. In the first three stages, maturation of gap junctional coupling was simulated by increasing PSC-CM patch conductivities from 10% to 40% and 100% of non-infarcted myocardium. In the final maturation stage, membrane kinetics and conductivities in the PSC-CM patch were represented by that of non-infarcted myocardium. (*B, D*) VT burden across stages of simulated PSC-CM patch maturation in (*B*) P1 and (*D*) P2 for remuscularization locations L1 (left) and L2 (right). (*C, E*) Number of distinct VT morphologies across stages of simulated patch maturation in (*D*) P1 and (*E*) P2 for locations L1 (left) and L2 (right).

was observed. At L2, only a single VT morphology was observed across all stages 1 through 3 (*Figure 6E*, right). The frequency of specific VT morphologies across maturation stages for remuscularization sites L1 and L2 in P1 (*Figure S6A*) and P2 (*Figure S6B*) can be found in the Supplementary material online.

These results indicate again that the site of remuscularization is an important determinant in the dynamics of VT burden during PSC-CM patch maturation. Across both patients and remuscularization sites, complete PSC-CM patch maturation (i.e. stage 4) dramatically reduced VT burden. VT burden was even completely alleviated at the appropriate remuscularization site.

4. Discussion

This study provides a broad *in silico* investigation of the arrhythmia consequences of direct remuscularization in two biophysically detailed,

personalized human ventricular models of post-MI patients. Direct remuscularization was simulated with PSC-CM patches applied to the ventricular myocardium just beneath the epicardial surface. In this way, direct contact between host and graft myocardium would enable electromechanical integration of the graft. First, we determined whether VT would be driven by focal or re-entrant mechanisms. For the latter, various treatment conditions were studied in the 3D post-MI ventricle models including engraftment state (i.e. partial vs. complete), site of remuscularization along the infarct, myofibril orientation of PSC-CMs in patches, patch size (i.e. patch diameter vs. thickness), and patch maturation. The objective was not to do an exhaustive sweep of treatment conditions but rather to identify important parameters that could contribute to the emergence of graft-induced arrhythmias. To this end, VT burden in both post-MI models at baseline was quantified to establish a baseline that more accurately determined arrhythmogenicity across simulated remuscularization conditions. This particular step was imperative because remuscularization alters the patient-specific, 3D structure of

surviving myocardial pathways around the infarct which have been previously shown to play an important role in VT.[28,50,51] We report here several key findings.

The first is that a re-entrant VT mechanism dominates over a focal mechanism in patch remuscularization. This was highlighted by two observations. First, PSC-CMs in an isolated myocardial patch were sufficiently coupled such that spontaneous beating would occur in a synchronous manner with beats emerging every ~1.6 s (37.5 b.p.m.) as commonly observed *in vitro*. Secondly, graft myocardium comprised of PSC-CMs would beat at only a fraction of this rate when coupled to host ventricular myocytes. The emergence and rate of spontaneous graft-induced ectopic propagations were dictated in part by source-sink effects between the host and graft myocardium; the host myocardium acted as an electrotonic sink to suppress PSC-CM automaticity within the graft. Specifically, we highlighted how increasing graft surface area interfacing with host myocardium as well as increasing electrotonic coupling between PSC-CMs in the graft reduced the frequency of and even completely suppressed graft-induced ectopic beats; both of these enhanced the ability of the host myocardium to suppress PSC-CM automaticity within the graft. Consequently, thin myocardial patches never spontaneously beat when fully engrafted. Even if they did, resting sinus rate (~60 b.p.m.) would override the slower rate of emergent graft-induced ectopic propagations. Thus, our results indicated that re-entrant as opposed to focal drivers would underlie VT in patch remuscularization.

This is in stark contrast to the recent observations that transient graft-induced VTs that emerge following PSC-CM injection are focal in nature. This is supported by two observations: (i) clinical pacing maneuvers were unable to terminate VTs and (ii) ectopic beats were observed to originate from sites of engrafted PSC-CMs.[23,26] While it has been proposed that PSC-CM automaticity due to immature membrane kinetics is to blame, how focal VTs *in vivo* with rates of >240 b.p.m. arise from PSC-CMs that spontaneously beat <60 b.p.m. *in vitro* remains an outstanding question. It is believed that the decline of PSC-CM automaticity due to *in vivo* maturation contributes to the reduction of the frequency and severity of VTs. Similar graft-induced VTs have not been observed or reported with transplantation of PSC-CM patches to date, however.[17,52]

Thus, we propose an alternative hypothesis for graft-induced VTs following PSC-CM injection in the light of a fundamental difference between remuscularization via cell injection vs. patch—that is the degree of electrotonic coupling. In cell injection, electromechanical junctions are just being established between both individual PSC-CMs and PSC-CMs and host ventricular myocytes. In patch remuscularization however, electromechanical junction formation occurs between PSC-CMs and host myocytes because PSC-CMs have been allowed to couple *in vitro*. Moreover, electrotonic coupling between PSC-CMs in myocardial patches is sufficient to maintain synchronous spontaneous beating. This is not the case following PSC-CM injection, however. Following their injection *in vivo*, PSC-CMs would beat dyssynchronously because they are poorly coupled and exhibit heterogeneous membrane kinetics. The dyssynchrony of PSC-CMs within a graft or between grafts could transiently give rise to fast-rate focal ectopic propagations that are not observed in our simulations. As electromechanical coupling improves however, we believe that the rate of persistent graft-induced focal ectopic beats would slow—similar to what we observe in our simulations. When slowed however, the interaction of graft-induced ectopic beats with sinus beats could initiate re-entry. The fundamental VT mechanism could therefore reasonably shift—from a graft-induced focal driver (as currently hypothesized) to a graft-induced, focal trigger but re-entrant

driver. To date, large animal studies that have investigated transient VT after PSC-CM injection into the post-MI ventricles have only done so at a snapshot in time when VTs were the most widespread (i.e. approx. 10 days following injection).[23,26] VTs were observed to persist up to more than several weeks in some of the animals. With improved PSC-CM electromechanical integration, these VTs could reasonably transition from a focal to a re-entrant driver mechanism. This could further explain why VT persists for significantly longer in some animals as opposed to others. Regardless, quantitative electrophysiological assessment of PSC-CM engraftment *in vivo* combined with more biophysically detailed simulations that better model discontinuous wave propagation is needed to validate this hypothesis; this remains particularly challenging experimentally, however.[53]

In addition to altering the emergence of graft-induced spontaneous ectopic propagations, the second main finding is that electrotonic interaction between the host and graft modulates electrical conduction through the latter. This was highlighted by two observations. First, electrical conduction through the patch as well as between the host and patch was slowed when engraftment was incomplete; conduction slowing could be especially noticeable at low host–graft conductivities. When engraftment was complete however, CV through the patch increased despite the fact that electrical conductivity in the patch remained unchanged. Thus, conduction slowing arising from partial PSC-CM patch engraftment can be particularly arrhythmogenic, highlighting the fact that there would be a vulnerable window during the early stages of patch integration. Secondly, CV through the patch was also reduced when patch thickness was increased to 1 and 2 mm. Increasing patch thickness had the effect of reducing the electrotonic effect of the host myocardium; in thinner patches, the rapid electrical propagation of the underlying host myocardium accelerated and drove electrical conduction across the patch. Slowed conduction across the patch arising from increasing patch thickness had the effect of increasing VT inducibility and thus VT burden. Re-entrant VTs could be a foreseeable complication of patch remuscularization, especially with thicker myocardial patches and when conduction velocities *in vitro* remain a fraction of what they are *in vivo*.[18] Although this result is more theoretical because patches of these thicknesses have yet to be consistently manufactured due to limitations in engineering vasculature,[54,55] it highlights how graft geometry can have an impact on electrical conduction. This also provides additional evidence for the likelihood of globular graft regions contributing to the emergence of re-entrant VT following PSC-CM injection at later stages of engraftment. The lack of graft-induced VTs with patch remuscularization[17,52] to date could potentially be attributed to the competing dynamics of graft survival vs. engraftment. We remain hopeful, however, that technical advances in tissue engineering and developmental biology will help address both the feasibility of creating larger myocardial tissues and those with more mature electromechanical properties.

The third main finding is that the patient-specific post-MI fibrotic substrate is a key factor in arrhythmogenicity in remuscularization with PSC-CM patches. Based on our study, individuals with large infarcts vulnerable to VT could be an ideal patient cohort. VT burden was almost always elevated in P2 but could be reduced in P1 under identical remuscularization conditions. Compared with P2, P1 had a much larger infarct. Infarct size alone is not an accurate indicator for VT vulnerability,[28] however. Additionally, the spatial distribution of scar and heterogeneous peri-infarcted tissue plays an important role. Despite this, infarct size could partially explain discrepancies across several pre-clinical large animal studies studying intramyocardial injection of PSC-CMs.[13,14,23,26] Highlighting this, Liu et al.[23] employed a large infarct model (25% of LV) and reported no

significantly elevated VT burden, while several other studies with smaller infarcts (~10% of LV) did.[13,14,26] An alternative contributing factor is that the methodology of inducing infarction impacts the distribution of scar and myocardial tissue that contribute to VT. While cryoinjury can more reasonably control for infarct geometry and size compared with coronary ligation,[27,56] fibrosis distribution of the healed infarct is less representative of ischaemia-reperfusion infarcts. All published large animal studies have utilized ischaemia-reperfusion to induce MI.[13,14,23,26] Because of the inconsistency in infarct geometry and size compounded by weak statistical power in most pre-clinical studies, however, comparison across pooled therapy and control groups is inadequate. Due to the potential life-threatening nature of VTs, we must ensure that direct remuscularization therapy does not elevate VT risk and VT burden for each treated individual as opposed to on average. Therefore, we propose that pre-clinical studies adopt a more rigorous methodology like the one that we describe here.

For realistic myocardial patch thicknesses, our fourth key finding is that the site of remuscularization is a critical determinant of VT burden once engraftment was complete. Other properties tested (myofibril orientation of patch PSC-CMs, patch size, and patch maturation) altered VT burden in a site-specific way. While certain locations were sensitive to patch conduction anisotropy and myofibre orientation, other sites were not. The sensitivity of a remuscularization site to patch myofibril orientation was patient specific. In P1, remuscularization directly over the infarct was not sensitive to patch myofibril orientation while it was in P2. Contrarily, P2 was not sensitive to patch myofibril orientation when remuscularization straddled infarcted and non-infarcted myocardium (i.e. L2) while it was in P1. Similarly, PSC-CM patch size altered VT burden in a site-dependent manner indicating that safe PSC-CM dosing in remuscularization requires one to consider the location of delivery. Surprisingly, inducibility and VT burden do not necessarily decrease with reduced remuscularization. Again, where PSC-CM patches are transplanted and allowed to engraft appears to play a critical role; patch radius did appear to positively correlate with severity or the number of distinct VT morphologies, however. Lastly, the dynamics of VT burden during simulated patch maturation was also site dependent. Complete patch maturation (i.e. stage 4) could alleviate VT burden when remuscularization occurred at specific locations (L1 in P1 and L2 in P2). The site dependence of arrhythmogenicity reinforces the importance of local conduction slowing and electrophysiological heterogeneity in determining VT burden and risk.[57] How graft myocardium alters these two in the patient-specific substrate, in both the acute and chronic setting, plays an important role in determining arrhythmogenicity. Highlighting this is that PSC-CM patches did not necessarily need to be mature, both ionically and electrotonically, if delivered to appropriate site in the appropriate patient (i.e. L1 in P1). Despite the many factors contributing to graft-induced arrhythmias, our result also highlights the potential for remuscularization to both treat HF progression and VT post-MI.

Consistent electromechanical engraftment of myocardial patches remains an experimental challenge. Details regarding how subepicardial access to the myocardium in several published studies reporting electromechanical engraftment[17,20] remains vague. A layer of epicardial fibrosis in several rat studies has been observed to inhibit electrotonic coupling between graft and host myocardium.[21,22,38,58] There are several reasons for how this could have arisen. First, sutures were used to attach the patches to the epicardium. This anchoring approach itself could contribute to scarring. Additionally, this methodology could also be inadequate in anchoring the patch to the epicardial surface giving rise to shearing at the host–graft interface with each ventricle contraction. Suture-free

anchoring approaches[43,59] could be explored to address this. For example, engineered myocardial tracts glued to the epicardial surfaces of the atria and ventricles were reported to restore atrioventricular conduction in a rat model of complete heart block.[43] Outside of strategies to accelerate engraftment, conductive biomaterials that help support physiological electrical conduction could be deployed[60,61] to mitigate VTs, whether transient or persistent. VT risk could also be mitigated by only treating patient cohorts with implantable cardioverter defibrillators. Lastly, physiological and pathophysiological tissue heterogeneity at the epicardium provides opportunities but also challenges to PSC-CM patch engraftment. Epicardial fat,[62] especially its prevalence in the healed infarct,[63] could limit where PSC-CM patch can be implanted along the infarct for example. However, recruitment and activation of epicardial cells appears to play a pivotal role in not just infarct healing but the potential to promote myocardial regeneration.[64–66]

Our long-term objective is to identify remuscularization strategies for post-MI patients that are not only non-arrhythmogenic but can be used to eliminate scar-related, re-entrant VTs. This is a particularly challenging multifactorial optimization problem—where one seeks to optimize mechanical contractility constrained to arrhythmia risk. In an initial proof of concept, we demonstrated that the patient-specific post-MI substrate is a contributing factor in arrhythmia following direct remuscularization indicating that patient risk stratification is imperative. Additionally, we demonstrated that partial engraftment of PSC-CM patches is particularly arrhythmogenic. When engraftment was complete, the site of remuscularization was critical in determining VT burden in PSC-CM remuscularization. Much like ablation therapies for treating VT,[31] remuscularization sites will require optimization. Overall, our study makes an important contribution in understanding VT dynamics in remuscularization of the post-MI ventricles with PSC-CMs and establishes a framework to assess clinical safety and initial steps towards patient-specific optimization of targeted remuscularization.

4.1 Clinical Implications

The long-term arrhythmia consequences of remuscularizing the post-MI ventricles remain unexplored. The addition and engraftment of PSC-CMs can alter the native myocardial substrate by introducing new channels and layers of conducting cardiac muscle. We showed that the individual patient substrate post-MI is an important consideration for remuscularization with PSC-CM patches. New re-entrant pathways can be unmasked, and new pathways can be formed by muscular grafts with immature PSC-CM membrane kinetic properties and poor electrotonic coupling. Of all the tested variables, graft location contributed the most to altering re-entrant VT dynamics and VT burden. Consequently, unoptimized remuscularization location can give rise to VT despite complete maturation and engraftment. Taken altogether, our results indicate that patient risk stratification is needed to identify candidates for remuscularization and that the remuscularization site requires optimization. Moreover, VT burden can be reduced and potentially alleviated with optimized remuscularization in the appropriate patient.

4.2 Limitations

We assumed complete survival and homogeneous coupling of PSC-CMs in the patches. However, studies of *in vivo* transplantation of engineered PSC-CM myocardial tissues have reported up to 20% PSC-CM survival and engraftment[17,20]; the subsequent PSC-CM survival and subsequent spatial distribution were not reported. Real-time tracking of PSC-CM viability and quantitative electrophysiological assessments of

electromechanical coupling[67] *in vivo* remain quite limited. Of the millions of PSC-CMs transplanted, only a fraction survives and engrafts.[13,17,20] We also assumed homogeneous engraftment of PSC-CM patches to the host myocardium (i.e. either complete or partial). Heterogeneous engraftment is highly likely based on observations of heterogenous conduction across monolayers *in vitro* and differences in the microenvironment (i.e. vasculature density, extracellular matrix composition, trabecular structure) of scar, peri-infarct, and non-infarcted myocardium. Batch-to-batch variations and electrophysiological heterogeneity of PSC-CMs[68,69] have also previously been reported; however, technological advances have enabled more robust differentiation and purification of ventricular-like PSC-CM subtypes. Lastly, the ionic mechanisms underlying membrane kinetics changes that occur during PSC-CM maturation *in vivo*[13,23,24] and *in vitro*[38,47,48,70,71] have yet to be biophysically characterized; as such, we were unable to simulate intermediate stages of PSC-CM maturation let alone heterogeneous spatial distributions of maturing PSC-CMs observed *in vivo*. On a broader note, we are cognizant that patch engraftment and maturation are both incremental processes that occur simultaneously. Realistically, there would be intermediate stages of engraftment and maturation to the endpoints we studied. Our *in silico* experiments focused on characterizing endpoints in part because of the uncertainty regarding the temporal, let alone spatial, dynamics of both these processes (i.e. PSC-CM alignment, electrotonic coupling within the graft, host–graft coupling, and ionic maturation). Despite all of these uncertainties, the principled approach for evaluating the arrhythmogenicity of direct remuscularization outlined here remains a necessary improvement to current methodologies. Moreover, the modularity of our simulation framework[72] enables the rapid integration of new experimental details as they become available. This will enable us to help predict patient-specific outcomes to specific remuscularization treatment plans using a characterized batch of PSC-CMs.

Supplementary material

Supplementary material is available at *Cardiovascular Research* online.

Conflict of interest: None declared.

Data availability

The data underlying this article will be shared on reasonable request to the corresponding author.

References

1. Bergmann O, Zdunek S, Felker A, Salehpour M, Alkass K, Bernard S, Sjostrom SL, Szewczykowska M, Jackowska T, dos Remedios C, Malm T, Andrä M, Jashari R, Nyengaard JR, Possnert G, Jovinge S, Druid H, Frisén J. Dynamics of cell generation and turnover in the human heart. *Cell* 2015;**161**:1566–1575.
2. Bergmann O, Bhardwaj RD, Bernard S, Zdunek S, Barnabé-Heider F, Walsh S, Zupicich J, Alkass K, Buchholz BA, Druid H, Jovinge S, Frisén J. Evidence for cardiomyocyte renewal in humans. *Science* 2009;**324**:98–102.
3. Benjamin EJ, Virani SS, Callaway CW, Chamberlain AM, Chang AR, Cheng S, Chiuve SE, Cushman M, Delling FN, Deo R, de Ferranti SD, Ferguson JF, Fornage M, Gillespie C, Isasi CR, Jimenez MC, Jordan LC, Judd SE, Lackland D, Lichtman JH, Lisabeth L, Liu S, Longenecker CT, Lutsey PL, Mackey JS, Matchar DB, Matsushita K, Mussolino ME, Nasir K, O'Flaherty M, Palaniappan LP, Pandey A, Pandey DK, Reeves MJ, Ritchey MD, Rodriguez CJ, Roth GA, Rosamond WD, Sampson UKA, Satou GM, Shah SH, Spartano NL, Tirschwell DL, Tsao CW, Voeks JH, Willey JZ, Wilkins JT, Wu JH, Alger HM, Wong SS, Muntner P, American Heart Association Council on E, Prevention Statistics C, Stroke Statistics S. Heart disease and stroke statistics-2018 update: a Report From the American Heart Association. *Circulation* 2018;**137**:e67–e492.
4. Kittleson MM. Recent advances in heart transplantation. *F1000Res* 2018;**7**:1008.
5. Quiñones MJ, Leor J, Kloner RA, Ito M, Patterson M, Witke WF, Kedes L. Transplantation of fetal myocardial tissue into the infarcted myocardium of rat. A potential method for repair of infarcted myocardium? *Circulation* 1996;**94**:1394–1336.
6. Scorsin M, Hagege A, Vilquin JT, Fiszman M, Marotte F, Samuel JL, Rappaport L, Schwartz K, Menasche P. Comparison of the effects of fetal cardiomyocyte and skeletal myoblast transplantation on postinfarction left ventricular function. *J Thorac Cardiovasc Surg* 2000;**119**:1169–1175.
7. Rubart M, Pasumarthi KB, Nakajima H, Soonpaa MH, Nakajima HO, Field LJ. Physiological coupling of donor and host cardiomyocytes after cellular transplantation. *Circ Res* 2003;**92**:1217–1224.
8. Roell W, Lewalter T, Sasse P, Tallini YN, Choi BR, Breitbach M, Doran R, Becher UM, Hwang SM, Bostani T, von Maltzahn J, Hofmann A, Reining S, Eiberger B, Gabris B, Pfeifer A, Welz A, Willecke K, Salama G, Schrickel JW, Kotlikoff MI, Fleischmann BK. Engraftment of connexin 43-expressing cells prevents post-infarct arrhythmia. *Nature* 2007;**450**:819–824.
9. Klug MG, Soonpaa MH, Koh GY, Field LJ. Genetically selected cardiomyocytes from differentiating embronic stem cells form stable intracardiac grafts. *J Clin Invest* 1996;**98**:216–224.
10. Lian X, Hsiao C, Wilson G, Zhu K, Hazeltine LB, Azarin SM, Raval KK, Zhang J, Kamp TJ, Palecek SP. Robust cardiomyocyte differentiation from human pluripotent stem cells via temporal modulation of canonical Wnt signaling. *Proc Natl Acad Sci U S A* 2012;**109**:E1848–1857.
11. Lian X, Zhang J, Azarin SM, Zhu K, Hazeltine LB, Bao X, Hsiao C, Kamp TJ, Palecek SP. Directed cardiomyocyte differentiation from human pluripotent stem cells by modulating Wnt/beta-catenin signaling under fully defined conditions. *Nat Protoc* 2013;**8**:162–175.
12. Burridge PW, Matsa E, Shukla P, Lin ZC, Churko JM, Ebert AD, Lan F, Diecke S, Huber B, Mordwinkin NM, Plews JR, Abilez OJ, Cui B, Gold JD, Wu JC. Chemically defined generation of human cardiomyocytes. *Nat Methods* 2014;**11**:855–860.
13. Chong JJ, Yang X, Don CW, Minami E, Liu YW, Weyers JJ, Mahoney WM, Van Biber B, Cook SM, Palpant NJ, Gantz JA, Fugate JA, Muskheli V, Gough GM, Vogel KW, Astley CA, Hotchkiss CE, Baldessari A, Pabon L, Reinecke H, Gill EA, Nelson V, Kiem HP, Laflamme MA, Murry CE. Human embryonic-stem-cell-derived cardiomyocytes regenerate non-human primate hearts. *Nature* 2014;**510**:273–277.
14. Shiba Y, Gomibuchi T, Seto T, Wada Y, Ichimura H, Tanaka Y, Ogasawara T, Okada K, Shiba N, Sakamoto K, Ido D, Shiina T, Ohkura M, Nakai J, Uno N, Kazuki Y, Oshimura M, Minami I, Ikeda U. Allogeneic transplantation of iPS cell-derived cardiomyocytes regenerates primate hearts. *Nature* 2016;**538**:388–391.
15. Shiba Y, Fernandes S, Zhu WZ, Filice D, Muskheli V, Kim J, Palpant NJ, Gantz J, Moyes KW, Reinecke H, Van Biber B, Dardas T, Mignone JL, Izawa A, Hanna R, Viswanathan M, Gold JD, Kotlikoff MI, Sarvazyan N, Kay MW, Murry CE, Laflamme MA. Human ES-cell-derived cardiomyocytes electrically couple and suppress arrhythmias in injured hearts. *Nature* 2012;**489**:322–325.
16. Gepstein L, Ding C, Rahmutula D, Rehemedula D, Wilson EE, Yankelson L, Caspi O, Gepstein A, Huber I, Olgin JE. In vivo assessment of the electrophysiological integration and arrhythmogenic risk of myocardial cell transplantation strategies. *Stem Cells* 2010;**28**:2151–2161.
17. Gao L, Gregorich ZR, Zhu W, Mattapally S, Oduk Y, Lou X, Kannappan R, Borovjagin AV, Walcott GP, Pollard AE, Fast VG, Hu X, Lloyd SG, Ge Y, Zhang J. Large cardiac muscle patches engineered from human induced-pluripotent stem cell-derived cardiac cells improve recovery from myocardial infarction in swine. *Circulation* 2018;**137**:1712–1730.
18. Kim DH, Lipke EA, Kim P, Cheong R, Thompson S, Delannoy M, Suh KY, Tung L, Levchenko A. Nanoscale cues regulate the structure and function of macroscopic cardiac tissue constructs. *Proc Natl Acad Sci U S A* 2010;**107**:565–570.
19. Montgomery M, Ahadian S, Davenport Huyer L, Lo Rito M, Civitarese RA, Vanderlaan RD, Wu J, Reis LA, Momen A, Akbari S, Pahnke A, Li RK, Caldarone CA, Radisic M. Flexible shape-memory scaffold for minimally invasive delivery of functional tissues. *Nat Mater* 2017;**16**:1038–1046.
20. Weinberger F, Breckwoldt K, Pecha S, Kelly A, Geertz B, Starbatty J, Yorgan T, Cheng KH, Lessmann K, Stolen T, Scherrer-Crosbie M, Smith G, Reichenspurner H, Hansen A, Eschenhagen T. Cardiac repair in guinea pigs with human engineered heart tissue from induced pluripotent stem cells. *Sci Transl Med* 2016;**8**:363ra148.
21. Jackman CP, Ganapathi AM, Asfour H, Qian Y, Allen BW, Li Y, Bursac N. Engineered cardiac tissue patch maintains structural and electrical properties after epicardial implantation. *Biomaterials* 2018;**159**:48–58.

22. Riegler J, Tiburcy M, Ebert A, Tzatzalos E, Raaz U, Abilez OJ, Shen Q, Kooreman NG, Neofytou E, Chen VC, Wang M, Meyer T, Tsao PS, Connolly AJ, Couture LA, Gold JD, Zimmermann WH, Wu JC. Human engineered heart muscles engraft and survive long term in a rodent myocardial infarction model. *Circ Res* 2015;**117**: 720–730.

23. Liu YW, Chen B, Yang X, Fugate JA, Kalucki FA, Futakuchi-Tsuchida A, Couture L, Vogel KW, Astley CA, Baldessari A, Ogle J, Don CW, Steinberg ZL, Seslar SP, Tuck SA, Tsuchida H, Naumova AV, Dupras SK, Lyu MS, Lee J, Hailey DW, Reinecke H, Pabon L, Fryer BH, MacLellan WR, Thies RS, Murry CE. Human embryonic stem cell-derived cardiomyocytes restore function in infarcted hearts of non-human primates. *Nat Biotechnol* 2018;**36**:597–605.

24. Cho GS, Lee DI, Tampakakis E, Murphy S, Andersen P, Uosaki H, Chelko S, Chakir K, Hong I, Seo K, Chen HV, Chen X, Basso C, Houser SR, Tomaselli GF, O'Rourke B, Judge DP, Kass DA, Kwon C. Neonatal transplantation confers maturation of PSC-derived cardiomyocytes conducive to modeling cardiomyopathy. *Cell Rep* 2017;**18**: 571–582.

25. Kadota S, Pabon L, Reinecke H, Murry CE. In vivo maturation of human induced pluripotent stem cell-derived cardiomyocytes in neonatal and adult rat hearts. *Stem Cell Rep* 2017;**8**:278–289.

26. Romagnuolo R, Masoudpour H, Porta-Sanchez A, Qiang B, Barry J, Laskary A, Qi X, Masse S, Magtibay K, Kawajiri H, Wu J, Valdman Sadikov T, Rothberg J, Panchalingam KM, Titus E, Li RK, Zandstra PW, Wright GA, Nanthakumar K, Ghugre NR, Keller G, Laflamme MA. Human embryonic stem cell-derived cardiomyocytes regenerate the infarcted pig heart but induce ventricular tachyarrhythmias. *Stem Cell Rep* 2019;**12**: 967–981.

27. Pecha S, Yorgan K, Rohl M, Geertz B, Hansen A, Weinberger F, Sehner S, Ehmke H, Reichenspurner H, Eschenhagen T, Schwoerer AP. Human iPS cell-derived engineered heart tissue does not affect ventricular arrhythmias in a guinea pig cryo-injury model. *Sci Rep* 2019;**9**:9831.

28. Arevalo HJ, Vadakkumpadan F, Guallar E, Jebb A, Malamas P, Wu KC, Trayanova NA. Arrhythmia risk stratification of patients after myocardial infarction using personalized heart models. *Nat Commun* 2016;**7**:11437.

29. Wit AL, Janse MJ. Experimental models of ventricular tachycardia and fibrillation caused by ischemia and infarction. *Circulation* 1992;**85**:I32–I42.

30. Kehat I, Khimovich L, Caspi O, Gepstein A, Shofti R, Arbel G, Huber I, Satin J, Itskovitz-Eldor J, Gepstein L. Electromechanical integration of cardiomyocytes derived from human embryonic stem cells. *Nat Biotechnol* 2004;**22**:1282–1289.

31. Prakosa A, Arevalo HJ, Deng D, Boyle PM, Nikolov PP, Ashikaga H, Blauer JJ, Ghafoori E, Park CJ, Blake RC, 3rd, Han FT, MacLeod RS, Halperin HR, Callans DJ, Ranjan R, Chrispin J, Nazarian S, Trayanova NA. Personalized virtual-heart technology for guiding the ablation of infarct-related ventricular tachycardia. *Nat Biomed Eng* 2018;**2**:732–740.

32. Bayer JD, Blake RC, Plank G, Trayanova NA. A novel rule-based algorithm for assigning myocardial fiber orientation to computational heart models. *Ann Biomed Eng* 2012;**40**:2243–2254.

33. ten Tusscher KH, Panfilov AV. Alternans and spiral breakup in a human ventricular tissue model. *Am J Physiol Heart Circ Physiol* 2006;**291**:H1088–H1100.

34. Vigmond EJ, Weber dos Santos R, Prassl AJ, Deo M, Plank G. Solvers for the cardiac bidomain equations. *Prog Biophys Mol Biol* 2008;**96**:3–18.

35. Vigmond EJ, Hughes M, Plank G, Leon LJ. Computational tools for modeling electrical activity in cardiac tissue. *J Electrocardiol* 2003;**36** Suppl:69–74.

36. Jincun G, Faguang Z, Weibin H, Yan W, Kang D, Tung R. Outside-in subepicardial dissection during percutaneous epicardial ventricular tachycardia ablation. *Circ Arrhythm Electrophysiol* 2016;**9**:e004499.

37. Shekar PS, Stone JR, Couper GS. Dissecting sub-epicardial hematoma—challenges to surgical management. *Eur J Cardiothorac Surg* 2004;**26**:850–853.

38. Shadrin IY, Allen BW, Qian Y, Jackman CP, Carlson AL, Juhas ME, Bursac N. Cardiopatch platform enables maturation and scale-up of human pluripotent stem cell-derived engineered heart tissues. *Nat Commun* 2017;**8**:1825.

39. Blazeski A, Lowenthal J, Zhu R, Ewoldt J, Boheler KR, Tung L. Functional properties of engineered heart slices incorporating human induced pluripotent stem cell-derived cardiomyocytes. *Stem Cell Reports* 2019;**12**:982–995.

40. Hsu EW, Muzikant AL, Matulevicius SA, Penland RC, Henriquez CS. Magnetic resonance myocardial fiber-orientation mapping with direct histological correlation. *Am J Physiol* 1998;**274**:H1627–H1634.

41. Roberts DE, Hersh LT, Scher AM. Influence of cardiac fiber orientation on wavefront voltage, conduction velocity, and tissue resistivity in the dog. *Circ Res* 1979;**44**: 701–712.

42. Paci M, Hyttinen J, Aalto-Setälä K, Severi S. Computational models of ventricular- and atrial-like human induced pluripotent stem cell derived cardiomyocytes. *Ann Biomed Eng* 2013;**41**:2334–2348.

43. Cingolani E, Ionta V, Cheng K, Giacomello A, Cho HC, Marban E. Engineered electrical conduction tract restores conduction in complete heart block: from in vitro to in vivo proof of concept. *J Am Coll Cardiol* 2014;**64**:2575–2585.

44. Vadakkumpadan F, Trayanova N, Wu KC. Image-based left ventricular shape analysis for sudden cardiac death risk stratification. *Heart Rhythm* 2014;**11**:1693–1700.

45. Cerqueira MD, Weissman NJ, Dilsizian V, Jacobs AK, Kaul S, Laskey WK, Pennell DJ, Rumberger JA, Ryan T, Verani MS, American Heart Association Writing Group on Myocardial Segmentation and Registration for Cardiac Imaging. Standardized myocardial segmentation and nomenclature for tomographic imaging of the heart. A statement for healthcare professionals from the Cardiac Imaging Committee of the Council on Clinical Cardiology of the American Heart Association. *Int J Cardiovasc Imaging* 2002;**18**:539–542.

46. Retuerto MA, Schalch P, Patejunas G, Carbray J, Liu N, Esser K, Crystal RG, Rosengart TK. Angiogenic pretreatment improves the efficacy of cellular cardiomyoplasty performed with fetal cardiomyocyte implantation. *J Thorac Cardiovasc Surg* 2004;**127**:1041–1049.

47. Ronaldson-Bouchard K, Ma SP, Yeager K, Chen T, Song L, Sirabella D, Morikawa K, Teles D, Yazawa M, Vunjak-Novakovic G. Advanced maturation of human cardiac tissue grown from pluripotent stem cells. *Nature* 2018;**556**:239–243.

48. Yoshida S, Miyagawa S, Fukushima S, Kawamura T, Kashiyama N, Ohashi F, Toyofuku T, Toda K, Sawa Y. Maturation of human induced pluripotent stem cell-derived cardiomyocytes by soluble factors from human mesenchymal stem cells. *Mol Ther* 2018; **26**:2681–2695.

49. Lemoine MD, Mannhardt I, Breckwoldt K, Prondzynski M, Flenner F, Ulmer B, Hirt MN, Neuber C, Horvath A, Kloth B, Reichenspurner H, Willems S, Hansen A, Eschenhagen T, Christ T. Human iPSC-derived cardiomyocytes cultured in 3D engineered heart tissue show physiological upstroke velocity and sodium current density. *Sci Rep* 2017;**7**:5464.

50. Jang J, Hwang HJ, Tschabrunn CM, Whitaker J, Menze B, Anter E, Nezafat R. Cardiovascular magnetic resonance-based three-dimensional structural modeling and heterogeneous tissue channel detection in ventricular arrhythmia. *Sci Rep* 2019;**9**: 9317.

51. Pashakhanloo F, Herzka DA, Halperin H, McVeigh ER, Trayanova NA. Role of 3-dimensional architecture of scar and surviving tissue in ventricular tachycardia: insights from high-resolution ex vivo porcine models. *Circ Arrhythm Electrophysiol* 2018;**11**: e006131.

52. Shudo Y, Miyagawa S, Ohkura H, Fukushima S, Saito A, Kawaguchi N, Matsuura N, Toda K, Sakaguchi T, Nishi H, Yoshikawa Y, Shimizu T, Okano T, Matsuyama A, Sawa Y. Adipose tissue-derived multi-lineage progenitor cells improve left ventricular dysfunction in porcine ischemic cardiomyopathy model. *J Heart Lung Transplant* 2017;**36**: 237–239.

53. Qin X, Han D, Wu JC. Molecular imaging of cardiac regenerative medicine. *Current Opin Biomed Eng* 2019;**9**:66–73.

54. Novosel EC, Kleinhans C, Kluger PJ. Vascularization is the key challenge in tissue engineering. *Adv Drug Deliv Rev* 2011;**63**:300–311.

55. Yang G, Mahadik B, Choi JY, Fisher JP. Vascularization in tissue engineering: fundamentals and state-of-art. *Prog Biomed Eng* 2020;**2**:012002.

56. van den Bos EJ, Mees BM, de Waard MC, de Crom R, Duncker DJ. A novel model of cryoinjury-induced myocardial infarction in the mouse: a comparison with coronary artery ligation. *Am J Physiol Heart Circ Physiol* 2005;**289**:H1291–H1300.

57. Liao SY, Tse HF, Chan YC, Mei-Chu Yip P, Zhang Y, Liu Y, Li RA. Overexpression of Kir2.1 channel in embryonic stem cell-derived cardiomyocytes attenuates posttransplantation proarrhythmic risk in myocardial infarction. *Heart Rhythm* 2013;**10**: 273–282.

58. Gerbin KA, Yang X, Murry CE, Coulombe KL. Enhanced electrical integration of engineered human myocardium via intramyocardial versus epicardial delivery in infarcted rat hearts. *PLoS One* 2015;**10**:e0131446.

59. Malki M, Fleischer S, Shapira A, Dvir T. Gold nanorod-based engineered cardiac patch for suture-free engraftment by near IR. *Nano Lett* 2018;**18**:4069–4073.

60. Mawad D, Mansfield C, Lauto A, Perbellini F, Nelson GW, Tonkin J, Bello SO, Carrad DJ, Micolich AP, Mahat MM, Furman J, Payne D, Lyon AR, Gooding JJ, Harding SE, Terracciano CM, Stevens MM. A conducting polymer with enhanced electronic stability applied in cardiac models. *Sci Adv* 2016;**2**:e1601007.

61. Pedrotty DM, Kuzmenko V, Karabulut E, Sugrue AM, Livia C, Vaidya VR, McLeod CJ, Asirvatham SJ, Gatenholm P, Kapa S. Three-dimensional printed biopatches with conductive ink facilitate cardiac conduction when applied to disrupted myocardium. *Circ Arrhythm Electrophysiol* 2019;**12**:e006920.

62. Iozzo P. Myocardial, perivascular, and epicardial fat. *Diabetes Care* 2011;**34** Suppl 2: S371–379.

63. Goldfarb JW, Roth M, Han J. Myocardial fat deposition after left ventricular myocardial infarction: assessment by using MR water-fat separation imaging. *Radiology* 2009; **253**:65–73.

64. Cao J, Poss KD. The epicardium as a hub for heart regeneration. *Nat Rev Cardiol* 2018;**15**:631–647.

65. Wei K, Serpooshan V, Hurtado C, Diez-Cunado M, Zhao M, Maruyama S, Zhu W, Fajardo G, Noseda M, Nakamura K, Tian X, Liu Q, Wang A, Matsuura Y, Bushway P, Cai W, Savchenko A, Mahmoudi M, Schneider MD, van den Hoff MJ, Butte MJ, Yang PC, Walsh K, Zhou B, Bernstein D, Mercola M, Ruiz-Lozano P. Epicardial FSTL1 reconstitution regenerates the adult mammalian heart. *Nature* 2015;**525**:479–485.

66. Bargehr J, Ong LP, Colzani M, Davaapil H, Hofsteen P, Bhandari S, Gambardella L, Le Novere N, Iyer D, Sampaziotis F, Weinberger F, Bertero A, Leonard A, Bernard WG, Martinson A, Figg N, Regnier M, Bennett MR, Murry CE, Sinha S. Epicardial cells derived from human embryonic stem cells augment cardiomyocyte-driven heart regeneration. *Nat Biotechnol* 2019;**37**:895–906.

67. Ransohoff KJ, Wu JC. Advances in cardiovascular molecular imaging for tracking stem cell therapy. *Thromb Haemost* 2010;**104**:13–22.

68. Zhu R, Millrod MA, Zambidis ET, Tung L. Variability of action potentials within and among cardiac cell clusters derived from human embryonic stem cells. *Sci Rep* 2016;**6**:18544.

69. Andersen P, Tampakakis E, Jimenez DV, Kannan S, Miyamoto M, Shin HK, Saberi A, Murphy S, Sulistio E, Chelko SP, Kwon C. Precardiac organoids form two heart fields via Bmp/Wnt signaling. *Nat Commun* 2018;**9**:3140.

70. Biermann M, Cai W, Lang D, Hermsen J, Profio L, Zhou Y, Czirok A, Isai DG, Napiwocki BN, Rodriguez AM, Brown ME, Woon MT, Shao A, Han T, Park D, Hacker TA, Crone WC, Burlingham WJ, Glukhov AV, Ge Y, Kamp TJ. Epigenetic priming of human pluripotent stem cell-derived cardiac progenitor cells accelerates cardiomyocyte maturation. *Stem Cells* 2019;**37**:910–923.

71. Hu D, Linders A, Yamak A, Correia C, Kijlstra JD, Garakani A, Xiao L, Milan DJ, van der Meer P, Serra M, Alves PM, Domian IJ. Metabolic maturation of human pluripotent stem cell-derived cardiomyocytes by inhibition of HIF1alpha and LDHA. *Circ Res* 2018;**123**:1066–1079.

72. Yu JK, Franceschi W, Huang Q, Pashakhanloo F, Boyle PM, Trayanova NA. A comprehensive, multiscale framework for evaluation of arrhythmias arising from cell therapy in the whole post-myocardial infarcted heart. *Sci Rep* 2019;**9**:9238.

Translational perspective

If safety from ventricular arrhythmias can be addressed, direct remuscularization with PSC-CMs—achieved either through engineered myocardial patches or intramyocardial injections—holds the potential to halt heart failure progression post-MI. Using personalized three-dimensional models of the post-MI ventricles derived from LGE-MRI, we provide evidence that arrhythmogenesis following remuscularization with PSC-CM patches is driven by a re-entrant as opposed to focal VT mechanism. Moreover, the existing patient-specific fibrotic substrate together with the remuscularization site was the primary determinant of arrhythmogenesis. These results suggest that the clinical safety of remuscularization can be achieved through patient-specific optimization guided in-part by computational modelling.